Uzbek Journal of Physics

Vol.20(№4) 2018 PP.209-217

STUDY OF NANOSTRUCTURES OF ZINC OXIDE SYNTHESIZED BY LOW-TEMPERATURE HYDROTHERMAL METHOD

S.S. Kurbanov, Sh.Z. Urolov, Z.Sh. Shaymardanov, R.R. Jalolov

Institute of Ion-Plasma and Laser Technologies of Uzbekistan Academy of Sciences, Tashkent, Uzbekistan, sskurbanov@gmail.com

Паст ҳароратда гидротермал усул ёрдамида синтез қилинган вертикал тартибли йўналган ва урчуқсимон, тартибсиз жойлашган рух оксиди (ZnO) нанородлари хона ҳароратида тадқиқ қилинган. Ҳавода вертикал йўналган ZnO нанородлари люминесценцияни қайд қилиш ўқига асосан параллел жойлашганда 382 нм тўлқин узунлигида жойлашган кучли ультрабинафша нурланиш полосасини намоён қилади. Бу полоса эркин экситонлар нурланишига нисбат берилган. Нанородлар ўсиш йўналиши билан люминесценцияни қайд қилиш ўқи орасидаги бурчак ошиб бориши билан 400 нм тўлқин узунлигида жойлашган янги бинафша люминесценция полосаси пайдо бўла бошлайди. Бу бинафша полоса нанородлар вакуумда ультрабинафша нур билан ёритилганда ҳам пайдо бўлади ва ҳаво таъсирида йўқолади. Тартибсиз жойлашган ZnO нанородларида эркин экситонга тегишли люминесценция полосаси билан бирга 590 нм тўлқин узунлигида жойлашган кенг сариқ-зарғалдоқ нурланиш ҳам кузатилади. Бинафша нурланиш полосаси Zn вакансиясига ёки унинг комплексларига тегишли нуқсонларга, сариқ-зарғалдоқ нурланиш эса тугунлар орасида жойлашган кислород атоми билан боғлиқ нуқсонларга нисбат берилган.

При комнатной температуре изучены фотолюминесцентные свойства вертикально ориентированных и веретенообразных, случайно ориентированных наностерженей ZnO, синтезированных с использованием низкотемпературного гидротермального метода. На воздухе вертикально ориентированные наностержни ZnO, расположенные в основном параллельно к оси регистрации люминесценции, проявляют только один сильный пик УФ-излучения при 382 нм. Эта полоса отнесена к излучению свободных экситонов. Новая фиолетовая полоса люминесценции около 400 нм возникает с увеличением угла между направлением роста наностержней и осью регистрации люминесценции. Фиолетовая полоса также появляется под УФ-освещением в вакууме и исчезает после воздействия воздуха. Случайно ориентированные наностержни ZnO, наряду с полосой люминесценции свободных экситонов, проявляют широкую желто-оранжевую полосу излучения около 590 нм. Фиолетовая полоса отнесена к дефектам, связанным с вакансиями Zn или их комплексами, тогда как желто-оранжевая полоса излучения отнесена к дефектам, связанным с междоузельным кислородом.

Room temperature photoluminescence (PL) properties of vertically aligned and spindle-shaped, randomly oriented ZnO nanorods synthesized by using a low temperature hydrothermal method are studied. In air, the vertically aligned ZnO nanorods oriented mainly parallel to the luminescence-recording axis exhibited only one, very strong UV emission peak at 382 nm. This band is assigned to emission of free excitons. A new violet PL band near 400 nm arises with increasing angle between the nanorod growth direction and the luminescence-recording axis. The violet band also appears under UV illumination in vacuum and vanishes after exposure to air. The randomly oriented ZnO nanorods along with free exciton related PL band reveal a broad yellow-orange emission band around 590 nm. The violet band is attributed to Zn vacancy related defects or their complexes, while the yellow-orange emission band is ascribed to oxygen interstitial related defects.

I. INTRODUCTION

In response to the ever-increasing energy demands and limited resources of traditional energy sources, on the one hand, and the concern for global warming, on the

other hand, environment-friendly and energy-efficient light sources, nanostructure materials based solar energy conversation elements have taken many researchers' attentions [1]. ZnO, being an important II-VI compound, has some superior physical and chemical properties, such as a direct wide band gap energy of ~3.37 eV, a large exciton binding energy of 60 meV at room temperature, it is particularly an attractive emitter in the violet and blue regions [2]. Furthermore, a very important characteristic of ZnO is its transparency in a wide range, good electronic conductivity, high chemical stability, non-toxicity, relatively simple and inexpensive technology for the synthesis of its various structures (nanocrystals, nanoparticles, thin films, etc.).

One-dimensional (1D) ZnO nanostructures with diversified morphology such as nanotubes, nanowires, nanobelts, and nanorods have been studied widely which can be used as potential building block in nanoelectronic and nanooptoelectronic devices [3, 4]. Specifically, ZnO nanorods in the form of hybrid or heterojunctions have shown extraordinary application prospects for photodetectors, gas sensors and photovoltaic devices in recent reports [5]. There are various methods for obtaining one-dimensional structures of zinc oxide, differing from each other by the synthesis temperature, the components used, the productivity, the cost, etc. A low-temperature solution approach offers the potential for a much-lowered fabrication cost and scale-up production, because it can eliminate the complicated issues associated with high-temperature manufacturing and vacuum processing. Moreover, the typical growth temperatures are below 100°C, allowing the fabrication even on substrates such as plastic, which is not allowed to be exposed to higher temperatures.

Usually, a photoluminescence (PL) spectrum of ZnO materials, as well as nanorods and nanoparticles, consists of two parts: a near band edge (NBE) emission centered at around 380 nm and a defect related deep level emission in the visible range. The defect related deep level emission depending on synthesis methods and post-grown treatment contains violet-blue (390–460 nm) or/and green (500–520 nm) or/and yellow-orange (560–600 nm) or/and red (650 nm) bands. The yellow-orange band has been ascribed to interstitial oxygen or complexes formed with oxygen [6-10]. It is frequently observed from ZnO nanomaterials grown from water-contained solutions of Zn compounds at relatively low temperatures.

On the contrary, the green band is often observed from ZnO materials fabricated in oxygen deficient conditions or after a high temperature annealing. It is attributed to oxygen vacancy defect centers [2, 11, 12]. The violet-blue emission could be separated into a violet band around 400 nm and a blue band at 420-460 nm. For the violet band a several emission mechanisms were proposed: zinc vacancy [10, 13-15], oxygen antisite (O_{Zn}) [16], and Zn interstitial (Zn_i) [17]. The deep level emission is a linkage channel for excitation. The relative intensity between the NBE and deep level emissions depends on the growth conditions, and it can be used as an indication of the optical quality of the structures.

In the present work, we have synthesized different 1D ZnO nanostructures using a low temperature hydrothermal method. Our studies show that PL spectra of the vertically aligned ZnO nanorods depend on nanorods spatial orientation relatively to luminescence-recording axis and ambient conditions. A violet band at ~400 nm was observed in vacuum or in air when nanorods growth direction was deviated from the luminescence-recording axis.

II. EXPERIMENTAL

ZnO nanostructures were synthesized through a low temperature hydrothermal route. The growth procedure was designed as follows: the aqueous solutions of zinc nitrate hexahydrate ($Zn(NO_3)_2 \cdot 6H_2O$) and hexamethyltetramine ($C_6H_{12}N_4$) were first prepared separately and then they were mixed together. The concentrations of both were fixed at 0.1 M. The mixture was stirred for 30 minute, yielding a clear and homogenous solution. The resulting suspension was transferred into a Teflon – lined stainless steel autoclave. Next, the pure and ITO film coated glass substrates with the ZnO seeding layer were dipped into the solution. The substrates with the ZnO seeding layer were placed face-down. Finally, the autoclave was sealed and put into the water thermostat bath. The hydrothermal reaction was carried out at 90°C for 5 hours.

Upon completion of the reactions, the autoclave cell was removed from the water thermostat bath instantly and allowed to cool down naturally, before the samples were removed from the autoclave. The samples were then washed in the deionized water several times and dried in air.

For the substrate pretreatment process, first pure and ITO film coated glass substrates were ultrasonically cleaned for 15 min in acetone and ethanol before spin coating. Then zinc acetate dihydrate ($Zn(CH_3COO)_2 \cdot 2H_2O$) was dissolved in pure ethanol at a concentration of 5 mM. This solution was coated several times onto substrates by a spin coater. The coated substrates were dried at room temperature and then annealed in air at 250°C for 30 min. The annealed temperature of 250°C is a little above the decomposition temperature of zinc acetate particles in order to form ZnO nanoparticles' seed layer.

The morphologies of the samples were investigated by using a scanning electron microscope (SEM) (PHILIPS XL-30). PL spectra were obtained employing a SPEX spectrometer equipped with a 0.75 m grating monochromator and lock-in technic, and an experimental setup consisting of a 0.75-m high-aperture monochromator and a BCI-280 boxcarintegrator designed to detect pulsed signals by the gating method. The samples were excited by a cw He-Cd laser (325 nm (3.812 eV), P~50 mW) and a pulsed N_2 laser (337 nm (3.68 eV), $\tau \sim 9$ ns, $P \sim 15$ kW, repetition rate of 100 Hz). A laser beams were focused on a ~125–150 μm spot through a long focal length UV lens. All measurements were performed in air at room temperature.

III. RESULTS AND DISCUSSION

Figure 1 shows the SEM micrographs of ZnO nanorods grown on the glass substrate with ZnO seed layer by the hydrothermal method. ZnO nanorods are vertically aligned and oriented perpendicularly to the substrate surface. The average length and diameter of the ZnO nanorods were found to be ~2–2.5 μm and 70–200 nm, respectively. The ZnO nanorod samples showed characteristic XRD peaks of hexagonal wurtzite crystal structure (not shown) and they were preferentially oriented along the (002) crystal plane.

Simultaneously with the vertically aligned ZnO nanorods grown on seeds, various nanostructures of ZnO were also deposited on glass, sapphire and silicon substrates placed on the bottom of the autoclave (Fig. 2). Depending on reaction temperature, duration and solution concentration the deposited nanostructures possesses different forms: spindle-shaped (*a*), flower-like structure composed of rods (*b*), flower-like structure composed of shaped pyramids (*c*) and dual hexagonal prisms (*d*). The individual

ZnO nanorods and shaped pyramids reveal the regular hexagonal structure. Spindle-shaped nanorods possess hexagonal form and their length and diameter are 18–20 and 0.5–1 μm, respectively. On the substrate, nanorods are located chaotically and have predominantly horizontal position. Some branches of flower-like ZnO nanostructures are single rods while the others consist of several rods.

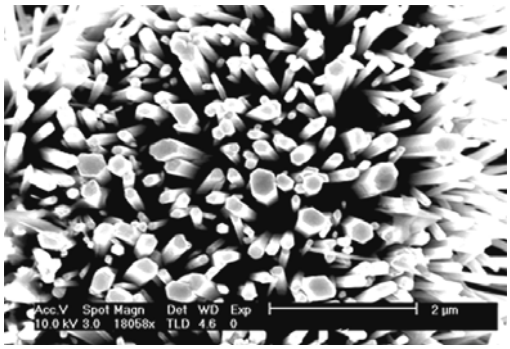

Fig. 1. SEM image of ZnO nanorods grown on glass substrates with the ZnO seeding layer.

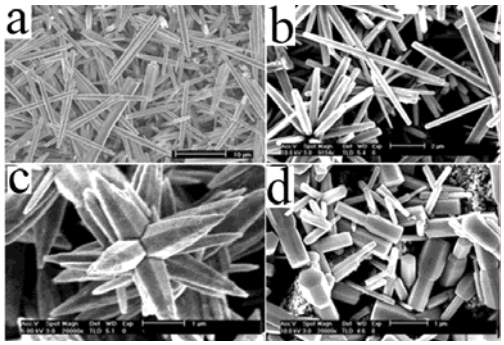

Fig. 2. SEM images of ZnO nanostructures deposited on glass substrates placed on the bottom of the autoclave: spindle-shaped (*a*), flower-like structure composed of rods (*b*), flower-like structure composed of shaped pyramids (*c*), dual hexagonal prisms (*d*).

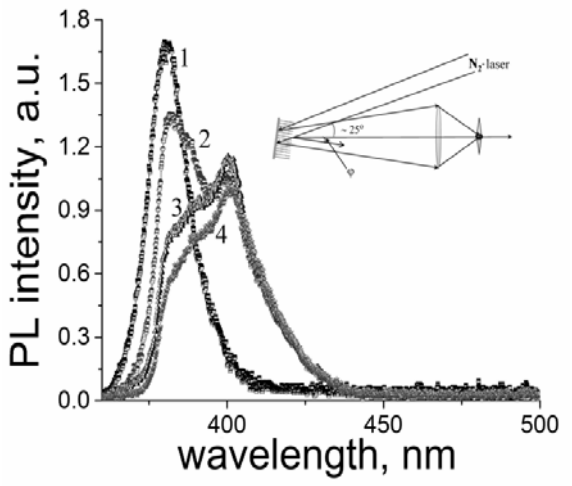

Fig. 3. Luminescence spectra of ZnO nanorods detected at different angles φ between the normal to the substrate surface with nanorods and the luminescence-recording axis: 0 (*1*), 20° (*2*), 35° (*3*) and 50° (*4*). The insert shows the luminescence-recording configuration of ZnO nanorods (φ is the angle between the normal to the substrate surface and the luminescence-recording direction).

Investigations showed that under UV irradiation aligned ZnO nanorods grown on seeds exhibit photoluminescence peaking at 382 nm. Figure 3 (curve *1*) shows the luminescence spectrum of ZnO nanorods recorded for the substrate oriented perpendicularly to the luminescence-recording axis. The PL spectrum contains only one peak. It is found that the spectrum and intensity of the luminescence depend on the detecting angle. With increasing the luminescence-recording angle (φ), a new PL band near 400 nm (violet band) appears, while the PL intensity starts to decrease. Figure 3 (curves *2-4*) shows the PL spectra acquired at φ = 20°, 35°, and 50°. Except for the luminescence spectrum obtained at φ=0, the other spectra can be presented as consisting of two Lorentzian components peaking at

~383 and ~401 nm (Fig. 4). The intensities of these components change oppositely with an increase in φ: the first band's intensity decreases, while the intensity of the second band increases. In other words, a redistribution of the luminescence total intensity between the UV and violet bands happens. And this in turn, leads to a decrease in the intensity ratio of the UV and emerging violet bands (Fig. 5).

It was found that the violet band could be revealed not only by rotating the nanorods: UV illumination of nanorods in vacuum also leads to an appearance of the violet emission band, even though the nanorods are oriented parallel to the luminescence-recording axis. In vacuum (~10^{-2} mm of Hg pressure) the UV peak intensity at ~380 nm grows almost three times, and a shoulder superimposed on the UV peak and extending up to 500 nm appears (Fig. 6, curve *2*)). After admission of air into the sample chamber, the UV peak intensity decreased only two times over a period of 1 h illumination, however, the PL spectrum did not recover its initial form. It is found that the recovering of the spectrum shape is a relatively slow process and takes a long time. Figure 6 (curve *3*) presents the PL spectrum of the ZnO nanorods detected after expose to air for 16 h. The emission spectrum of ZnO nanorods was once again recorded in vacuum ambient (Fig. 6, curve 4).

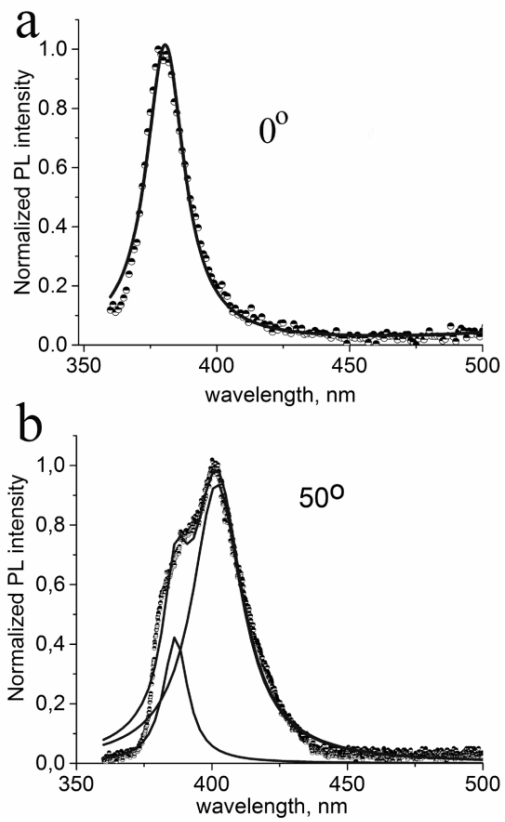

Fig. 4. Decomposition of the PL spectra of ZnO nanorods acquired under different angles (φ) into Lorentzian components: 0° (*a*) and 50° (*b*). Dots are experimental data, solid curves are Lorentzian components.

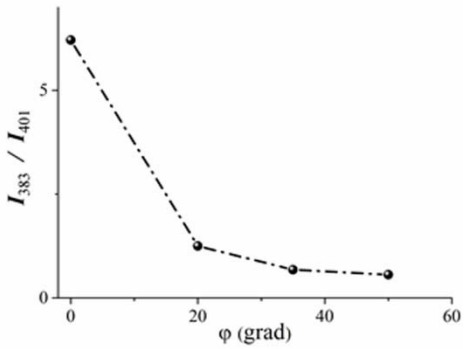

Fig. 5. Dependence of the intensity ratio of the PL bands on the detection angle.

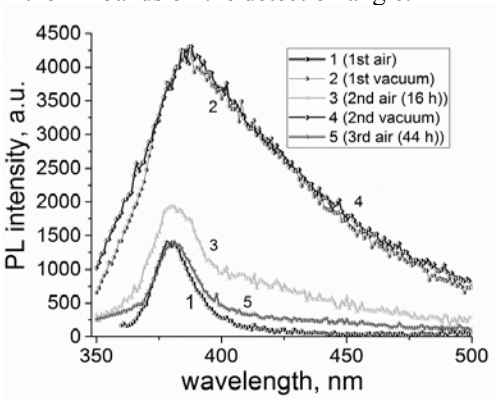

Fig. 6. Room temperature PL spectra for ZnO nanorods recorded in different ambient conditions: the first time in air (*1*), the first time in vacuum (*2*), the second time in air (*3*), the second time in vacuum (*4*), the third time in air (*5*), the third time in vacuum (*6*).

This spectrum is almost the same as that obtained in the first time in vacuum (curve *2*). Flooding the chamber with ambient air leads to the same response of the PL intensity, the UV peak intensity decreases ~2 times. In this case, the nanorods were kept in air more long time. Figure 6 (curve *5*) shows the PL spectrum recorded from the nanorods exposed to ambient air for 44 h. In comparison with the PL spectrum recorded after 16 h exposure to air, the obtained spectrum possesses the intense UV peak and the long wavelength shoulder intensity was reduced drastically.

The PL spectrum recorded in vacuum ambient can be divided into two Lorentzian bands located at ~384 nm (3.23 eV) and ~405 nm (3.06 eV) (Fig. 7*b*). According to the conventional classification for ZnO crystals, the sharp UV peak at around 382–384 nm can be assigned to a near band edge (NBE) emission (recombination of free ZnO excitons) [2]. Because the ZnO nanorods were synthesized without intentional doping, the violet band around 400 nm can be attributed to native defect related deep level emission centers. An appearance of the violet emission band only after UV illumination of the nanorods in vacuum indicates that under UV illumination the emission centers responsible for the violet band are created or existing centers become active. Considering the fact that the N_2 laser energy (3.68 eV) is not enough to create defect centers in ZnO, we can infer that an appearance of the violet band is due to activation of the existing emission centers.

Zn vacancies possess the lowest formation energy among the native point defects and they are more favorable in oxygen-rich conditions [18]. The hydrothermal method provides a growth of ZnO materials in O-rich conditions. Based on these facts we can attribute the observed violet emission band to Zn vacancy related defects: transitions of electrons from conducting band or shallow donor levels to neutral zinc vacancy could give rise to the violet luminescence.

Regarding the ambient condition's effect on the violet band appearance, we suggest that the UV illumination of the ZnO nanorods in vacuum gives rise to dissociation of V_{Zn}-H centers forming Zn vacancies and interstitial H atoms. A part of the released hydrogen atoms will move away from the V_{Zn} defects and leave the nanorod due to relatively low diffusion activation energy. This suggestion is based on first-principles calculations, where have been shown that H can passivate zinc vacancy defects in ZnO by forming strong O-H chemical bonds [19, 20]. First-principles calculations by Wardle et al. revealed that V_{Zn}-H is partially passivated with a (−/0) level at E_v+0.46 eV [21].

The observed detection angle dependence of the PL intensity and spectrum of the aligned nanorods can be caused by different special distribution of emission centers in ZnO nanorods. The exciton luminescence is known to be excited in the entire volume of nanorod, and most of it is channeled in a nanorod due to refractive index differences of ZnO (2.2) and surrounding air (1). As can be seen in (Fig. 3), at φ=0 the recoding system collects radiation basically emitted from nanorods end faces. In the turn, the violet PL band intensity increases with increasing φ. It means the violet band is weakly channelized and more light emerging from lateral nanorod surfaces falls into the monochromator slit (Fig. 8). It indicates that zinc vacancies must be localized predominantly in the near-surface layers of the nanorod. This suggestion is in good agreement with the data and conclusions of [22]. In this work, it was shown based on experimental data obtained using positron annihilation that the zinc vacancy centers are mainly located on the surface and/or in the surface region of zinc oxide structures and are more sensitive to surface effects.

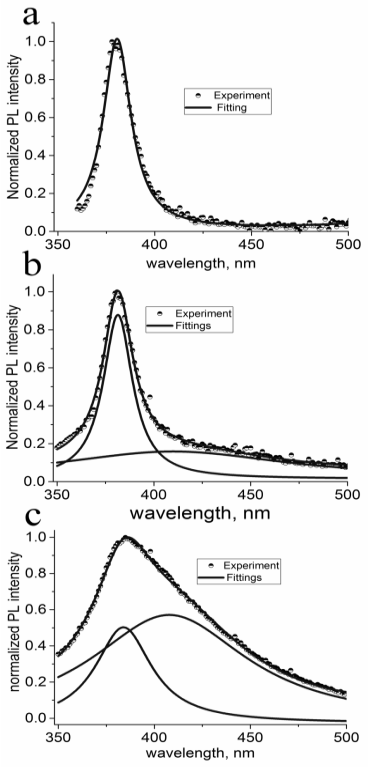

Fig. 7. Decomposition of the PL spectra of ZnO nanorod recorded in different ambient conditions into Lorentzian components: the first time in air (*a*), the first time in vacuum (*b*), in air (*c*), after 44 h when the PL measurements in vacuum were carried out.

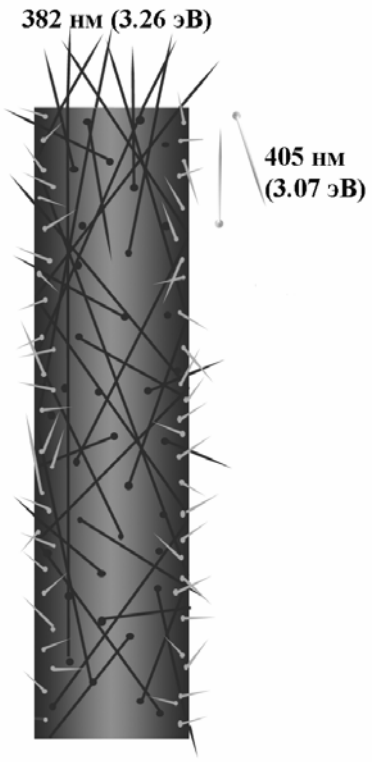

Fig. 8. Schematic illustration of emission centers distribution in the ZnO nanorod volume.

As was mentioned above the hydrothermal method provides a growth of ZnO materials in O-rich conditions and it is favor for formation of interstitial oxygen defect centers along with Zn vacancy related defects. Thus, ZnO structures grown by using the hydrothermal method would manifest an emission caused by the interstitial oxygen defect centers. In was found that at room temperature under UV irradiation (337 nm) as-grown ZnO spindle-shaped nanorods deposited on the substrates placed on the bottom of the autoclave also exhibit a photoluminescence (Fig. 9). The PL spectrum contains a sharp UV peak located around 390 nm (3.18 eV) and a broad emission band around 590 nm (2.1 eV). After annealing in air at 500°C for 1 h the UV peak intensity increased and instead of the PL band at 590 nm a new emission band located at 540 nm (2.3 eV) appeared. These PL bands were assigned to oxygen interstitial and oxygen vacancy related defects, respectively [6-12]. The thermoannealing results in an increase in the UV band intensity and growth of the relative peak intensity ratio of the UV band to the native defect related emission from ~2.3 to ~3.5. A high intensity of the near-band-edge emission and a weak deep-level emission is a criterion of the ZnO nanorods quality. These results are an indication of the improvement of the stoichiometric proportions and crystalline quality of the sample. We consider that the improvement occurred mostly as a

result of the release of oxygen interstitial atoms and concentration of the new created oxygen vacancy related centers is no so much.

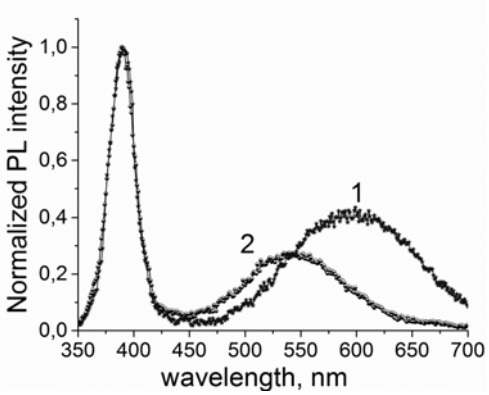

Fig. 9. Room temperature PL spectra of as-grown (1) and high temperature annealed (2) ZnO spindle-shaped nanorod samples.

The differences in the UV emission peak positions of the vertically grown and randomly deposited ZnO nanorods could be related to the different dimensions of the ZnO nanorods or laser excitation heating effect of the sample [23]. It can be seen from Fig. 2(a) spindle-shaped nanorods possess a larger diameter with respect to the vertically aligned one (Fig. 1). An average diameter of the randomly deposited ZnO nanorods is almost 5-6 times larger than that of the aligned nanorods. As was mentioned above zinc vacancy centers are predominantly localized in the near-surface layers of the nanorod and this statement is confirmed by the detection angle dependent measurements of the luminescence spectrum. In contrary as was reported [24], the yellow-orange luminescence from ZnO structures was not sensitive to the surface modifications of the nanostructures and could be originated from the defects localized in the bulk, not on the surface. Thus, changes in the surface-to-volume ratio of ZnO structures, as well as nanorods should affect the violet and yellow-orange luminescence intensities in the opposite directions. For a rod of height h and radius r, the surface-to-volume ratio R can be expressed as

$$R = \frac{S}{V} = \frac{2\pi r^2 + 2\pi rh}{\pi r^2 h}.$$

For the vertically grown ZnO nanorods the surface-to-volume ratio is ~30, while for the randomly deposited ZnO nanorods it is equal to ~6. Obviously, the vertically grown nanorods have more advanced surface but small volume than that the randomly deposited nanorods and the yellow-orange luminescence band will dominate in the PL spectrum ascribed from the randomly deposited ZnO nanorods.

IV. CONCLUSIONS

We synthesized vertically aligned as well as spindle-shaped, randomly oriented ZnO nanorods by using the low temperature hydrothermal method. Under UV irradiation in air, the vertically aligned nanorods exhibit a PL at 382 nm when they are oriented mainly parallel to the luminescence-recording axis. In air, with increasing the angle between the nanorod growth direction and the luminescence-recording axis a violet PL band near 400 nm arises. This band also appears under UV illumination in vacuum and vanishes after exposure to air. The PL band at 382 nm is assigned to emission of free excitons, whereas the violet band is attribute to zinc vacancy defects. The dependence of the luminescence spectrum of ZnO nanorods on their spatial orientation may be related to the localization of zinc vacancies in the nanorod surface layer. The observed effect of the ambient conditions on the PL spectrum indicates that the UV illumination in vacuum could result

in dissociation of the hydrogen passivated V_{Zn}-H centers into zinc vacancies and interstitial hydrogen atoms. ZnO spindle-shaped randomly oriented nanorods along with free exciton related PL band exhibit a broad emission band at around 590 nm (2.1 eV). Taking into account that the deep level related PL bands were detected from the ZnO nanorods grown in oxygen-rich conditions the yellow–orange broad emission band is ascribed to oxygen interstitial related defects. Detection of the yellow–orange PL band from spindle-shaped randomly oriented nanorods could be elucidated by different features of the vertically aligned and randomly oriented ZnO nanorods. Namely, the vertically grown nanorods have more advanced surface but small volume than that the randomly oriented nanorods and in the latter the yellow–orange PL band dominates over the violet emission due to belonging it to defects localized in the bulk.

Acknowledgments. This work was supported by the State Program for Basic Research of Republic of Uzbekistan (OT-F2-52).

REFERENCES

1. Q. Dai, C.E. Duty, M.Z. Hu, Small **6**, 1577 (2010).
2. Ü. Özgür, Ya.I. Alivov, C. Liu, A. Teke, M.A. Reshchikov, S. Doğan, V. Avrutin, S.-J. Cho, H. Morkoç, J. Appl. Phys. **98**, 041301 (2005).
3. H.P. Tang, H. Li, H.P. He, Mater. Lett. **158**, 80 (2015).
4. X.D. Meng, B.X. Lin, B.J. Gu, J.J. Zhu, Z.X. Fu, Solid State Commun. **135**, 411 (2005).
5. N. Gogurla, S.C. Kundu, S.K. Ray, Nanotechnology **28**, 145202 (2017).
6. L. Wu, L. Wu, X. Pan, F. Kong, Opt. Mater. **28**, 418 (2006).
7. J.W.P. Hsu, D.R. Tallant, R.L. Simpson, N.A. Missert, R.G. Copeland, Appl. Phys. Lett. **88**, 252103 (2006).
8. A.B. Djurišić, Y.H. Leung, K.H. Tam, L. Ding, W.K. Ge, H.Y. Chen, S. Gwo, Appl. Phys. Lett. **88**, 103107 (2006).
9. X. Liu, X. Wu, H. Cao, R.P.H. Chang, J. Appl. Phys. **95**, 3141 (2004).
10. X.L. Wu, G.G. Siu, C.L. Fu, H. C. Ong, Appl. Phys. Lett. **78**, 2285 (2001).
11. K. Vanheusden, W.L. Warren, C.H. Seager, D.R. Tallant, J.A. Voigt, J. Appl. Phys. **79**, 7983 (1996).
12. F.H. Leiter, H.R. Alves, A. Hofstaetter, D.M. Hofmann, B.K. Meyer, Phys. Status Solidi (b) **226**, R4 (2001).
13. S.H. Jeong, B.S. Kim, B.S. Lee, Appl. Phys. Lett. **82**, 2625 (2003).
14. G. Hua, Y. Zhang, Ch. Ye, M. Wang, L. Zhang, Nanotechnology **18**, 145605 (2007).
15. S.S. Kurbanov, G.N. Panin, T.W. Kim, T.W. Kang, J. Luminescence **129**, 1099 (2009).
16. Q.X. Zhao, P. Klason, M. Willander, H.M. Zhong, W. Lu, J.H. Yang, Appl. Phys. Lett. **87**, 211912 (2005).
17. B. Kumar, B. Gonga, S. Vicknesh, S.J. Chua, S. Tripathy, Appl. Phys. Lett. **89**, 141901 (2006).
18. A. Janotti, C.G. Van deWalle, Rep. Prog. Phys. **72**, 126501 (2009).
19. C.G. Van de Walle. In Proceedings of the 1st International Workshop on Hydrogen in Materials and Vacuum Systems, G.R.Myneni and Chattopadhyay, Eds., of AIP Conference Proceedings, **671**, 33 (2003).
20. A. Janotti, C.G. Van de Walle, Phys. Rev. B **76**, 165202 (2007).
21. M.G. Wardle, J.P. Goss, P.R. Briddon, Phys. Rev. B **72**, 155108 (2005).
22. A. Zubiaga, F. Tuomisto, F. Plazaola, K. Saarinen, J.A. Garcia, J.F. Rommeluere, J. Zuniga-Perez, and V. Munoz-Sanjose, Appl. Phys. Lett. **86**, 042103 (2005).
23. S.S. Kurbanov, Kh.T. Igamberdiev, T.W. Kang, J. Phys. D: Appl. Phys. **43**, 115401 (2010).
24. D. Li, Y.H. Leung, A.B. Djurišić, Z.T. Liu, M.H. Xie, S.L. Shi, S.J. Xu, W.K. Chan, Appl. Phys. Lett. **85**, 1601 (2004).